ISIJ International, Vol. 46 (2006), No. 4, pp. 490–495

Reaction Mechanism between Solid CaO and FeO_x–CaO–SiO_2–P_2O_5 Slag at 1 573 K

Tasuku HAMANO, Shinya FUKAGAI and Fumitaka TSUKIHASHI

Department of Advanced Materials Science, Graduate School of Frontier Sciences, The University of Tokyo, Kashiwa, Chiba 277-8561 Japan.

(*Received on October 19, 2005; accepted on January 13, 2006*)

Solid CaO and FeO_x–CaO–SiO_2–P_2O_5 slag were reacted for 2 to 2 400 s at 1 573 K. The interface of CaO and slag were observed and analyzed by SEM/EDS. The CaO–FeO layer was formed beside solid CaO. The thickness of the CaO–FeO layer increased with time. Next to the CaO–FeO layer, $2CaO \cdot SiO_2$ phase was formed in the melt and high content of FeO was included in the liquid. The activities of FeO and CaO for each phase were evaluated and reaction mechanism between solid CaO and FeO_x–CaO–SiO_2–P_2O_5 slag was discussed. The activity of FeO for $2CaO \cdot SiO_2$ saturated melt is larger than that for the CaO–FeO layer, therefore, Fe^{2+} diffuses from slag phase to solid CaO. Then the CaO–FeO layer is formed beside solid CaO. The pass of the slag composition change accompanied by CaO dissolution are represented in the phase diagram for the FeO_x–CaO–(SiO_2+P_2O_5) pseudo ternary system.

KEY WORDS: CaO; dissolution; hot-metal; dephosphorization; FeO_x–CaO–SiO_2–P_2O_5 system; multi-phase flux.

1. Introduction

The hot-metal dephosphorization process has been developed to meet increasing requirements for the production of low-phosphorus steel over the last couple of decades. The basic flux is required for effective dephosphorization. Therefore, the CaO-based slag containing iron oxide is often used in this process. The FeO_x–CaO–SiO_2–P_2O_5 system is the typical slag for steelmaking coexisting solid and liquid phases at the hot-metal temperatures. A lot of researches on hot-metal dephosphorization reaction has been conducted, however, in most cases, the slag is treated as homogeneous liquid slag and the contribution of solid phase, undisolved CaO and calcium silicate phase such as $2CaO \cdot SiO_2$, to dephosphoriazation is not taken into account. Recently, it is required to reduce the amount of steelmaking slag production because of the environmental issues. It is one of the effective methods for reducing steelmaking slag emission to increase the efficiency of utilization of CaO reaction. Thus it is important to reveal the reaction mechanism of CaO dissolution into slag. It is well known that calcium silicate and calcium phosphate form stable solid solution or compound at hot-metal temperatures. Therefore, if phosphorus in the slag were condensed in the solid calcium silicate phase, it would be possible to use the solid phase including multi-phase flux to the hot-metal dephosphorization process. Several investigations have been carried out for the reaction of solid CaO and slag,[1–13] however, the mechanism of reaction is not yet fully clarified.

In the present study, solid CaO piece and FeO_x–CaO–SiO_2–P_2O_5 slag were reacted at 1 573 K. The interface of CaO and slag were observed and analyzed by SEM/EDS. The microscopic behavior of phosphorus in the multi-phase flux was investigated and the reaction mechanism between solid CaO and FeO_x–CaO–SiO_2–P_2O_5 slag was discussed.

2. Experimental

The electric furnace with $MoSi_2$ heater and mullite reaction tube (outer diameter: 70 mm, inner diameter: 63 mm, length: 1000 mm) was employed. The slag sample was prepared by mixing the synthesized wustite (Fe_tO), CaO, reagent grade SiO_2 and $3CaO \cdot P_2O_5$. A CaO piece of about 3 g was cut from a sintered CaO crucible (purity: 99.9%, density: 3.3×10^3 kg/m^3) and used for solid CaO sample. The oxygen partial pressure was controlled by CO–CO_2 mixture. Both CO and CO_2 gas were dehydrated by passing through silicagel, and soda lime was also used to remove CO_2 in CO gas. In this study, mixture ratio of CO/CO_2 was 100/1 and the oxygen partial pressure was calculated to be 1.8×10^{-9} Pa from Eqs. (1) and (2).

$$CO\,(g) + \frac{1}{2} O_2\,(g) = CO_2\,(g) \quad \text{.....(1)}$$

$$\Delta G^\circ = -281\,000 + 85.2T \ \text{J/mol}^{14)} \quad \text{.....(2)}$$

Ten grams of slag sample charged in an alumina crucible (outer diameter: 38 mm, inner diameter: 34 mm, height: 45 mm) was set in the furnace and CO–CO_2 gas (CO/CO_2 = 100/1) was flown with 350 cm^3/min from top of the reaction tube. After 1 800 s, three grams of solid CaO piece was put in the crucible. If the reaction time was short-

er than 30 s, solid CaO sample was attached to the top of a mullite tube (outer diameter: 6 mm, inner diameter: 4 mm, length: 1 000 mm) by using alumina cement. The $CO–CO_2$ gas was stopped and high purity Ar was introduced from the bottom of the reaction tube, then CaO sample was dipped in the slag. After the reaction time, the CaO piece was quickly taken out from the furnace and quenched in flushing Ar. Then CaO sample was embedded in a polyester resin and polished using SiC abrasive paper. The interface of CaO and slag were observed by SEM and the reacted layers were analyzed by EDS. The slag sample was crushed for chemical analysis. The metallic iron in the slag sample was removed by magnetic separation before analysis. The content of Ca and Al were determined by ICP-AES. The gravimetry was applied for SiO_2 analysis. The total iron and the Fe^{2+} content were determined by the titration method using $K_2Cr_2O_7$ and Fe^{3+} content was calculated. Phosphorus contents were analyzed by molybdenum blue colorimetry.

3. Results and Discussion

Since the FeO_x containing slag and carbon saturated molten iron are reacted in the practical hot-metal dephosphorization process, the oxygen partial pressure in the system is very low. In the present study, the oxygen partial pressure was controlled by using $CO–CO_2$ mixture, therefore, the initial slag is required to be the same composition. The Fe^{3+}/Fe^{2+} ratio is affected by oxygen partial pressure. Thus preliminary experiment was carried out to investigate changes of slag composition with time. The initial slag is 25.3mass%FeO_x–30.8mass%CaO–33.1mass%SiO_2–10.8mass%P_2O_5 system. Seven grams of slag sample was charged in an alumina crucible and kept for 0 to 14 400 s with controlled oxygen partial pressure of 1.8×10^{-9} Pa at 1 573 K. After the experiment, the sample with the crucible was quenched by flushing Ar and crushed for chemical analysis. The results of slag composition are shown in **Table 1**. The iron oxides content decreased with increasing experimental time and the Fe^{3+}/Fe^{2+} ratio also decreased with time. As the wüstite was synthesized with the condition of solid iron coexistence, the equilibrium oxygen partial pressure was higher than that of experiments and the content of iron oxides decreased after the experiment. **Figure 1** shows the relationship between the Fe^{3+}/Fe^{2+} and experimental time. The Fe^{3+}/F^{2+} ratio decreased with time and it is constant after 1 800 s. Consequently, the slag was pre-melted for 1 800 s before experiments.

The solid CaO and FeO_x–CaO–SiO_2–P_2O_5 slag were reacted in an alumina crucible at 1 573 K for 2 to 2 400 s. The sample names are CS-2, CS-10, CS-20, CS-30, CS-300, CS-600, CS-1200 and CS-2400, where the numbers after hyphen mean the reaction time in seconds. **Figures 2**(a) to 2(h) demonstrate the SEM images of CaO-slag interface for samples (a) CS-2, (b) CS-10, (c) CS-20, (d) CS-30, (e) CS-300, (f) CS-600, (g) CS-1200 and (h) CS-2400. The numbers shown in Figs. 2(a) to 2(h) mean the positions analyzed by EDS. The results of EDS analysis for positions of samples CS-2 to CS-30 and those of samples CS-300 to CS-2400 are shown in **Tables 2** and **3**, where the iron oxide is calculated as FeO because the oxygen partial pressure during the experiment is low.

Table 1. Results of pre-melt slag analysis (mass%).

Sample	Experimental time (s)	FeO	Fe_2O_3	CaO	SiO_2	P_2O_5	Al_2O_3	Fe^{3+}/Fe^{2+}
PR-1	0	20.0	6.06	30.9	31.8	10.6	0.628	0.272
PR-2	900	16.7	5.82	32.6	31.7	11.6	1.65	0.313
PR-3	1800	22.0	2.21	31.2	30.4	10.9	3.28	0.0901
PR-4	3600	24.7	1.30	29.3	28.8	10.3	5.57	0.0476
PR-5	14400	19.7	1.83	31.2	30.1	10.3	6.91	0.0835

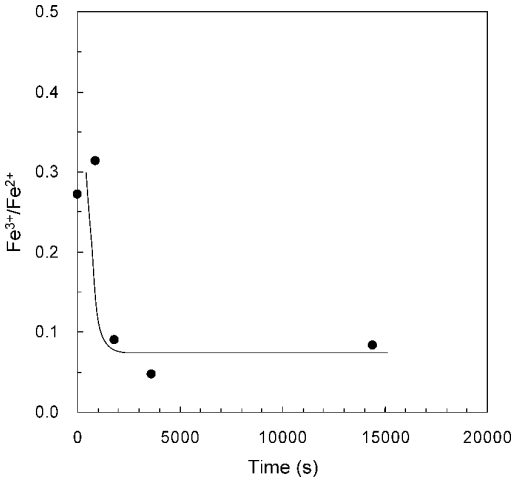

Fig. 1. Relationship between Fe^{3+}/Fe^{2+} ratio and experimental time.

The CaO–FeO layer was observed adjacent to solid CaO, and next to the CaO–FeO layer the CaO–SiO_2 or CaO–SiO_2–P_2O_5 phase with the FeO–CaO–SiO_2 melt were observed in each SEM image of Fig. 2. The composition of the positions in the CaO–FeO layer in Fig. 2, 2 and 3 in (a), 5 to 11 in (b), 3 to 5 in (c), 1 to 7 in (d), 2 and 3 in (e), 1 and 2 in (f), 1 to 3 in (g) and 2 and 3 in (h), were analyzed that SiO_2 is included less than 5 mass% and the ratio of CaO/FeO approximately equals unity. This suggests that $2CaO\cdot Fe_2O_3$ phase was formed in CaO–FeO layer. However, the $2CaO\cdot Fe_2O_3$ does not exist but 28mass%CaO–72mass%FeO liquid phase and CaO–10mass%FeO solid solution coexist at 1 573 K according to the phase diagram for CaO–FeO system.[15] Therefore, this phase seems to be formed during solidification.

In the Fig. 2, the positions 4, 5 and 7 to 9 in (a), 12 and 13 in (b), 6 and 7 in (c), 8 and 10 to 12 in (d), 4, 6 and 7 in (e), 3 to 6 in (f), 4 and 6 in (g) and 4 to 6 in (h) were identified as $2CaO\cdot SiO_2$ phase with 1 to 10 mass% P_2O_5. In addition, the positions in the CaO–SiO_2–P_2O_5 phase of Fig. 2, 16 in (b), 10 in (e), 7 and 11 in (g) and 7, 9 to 12 in (h), contain P_2O_5 of 15 to 25 mass%. These CaO–SiO_2–P_2O_5 phases close to $5CaO\cdot SiO_2\cdot P_2O_5$ or $7CaO\cdot 2SiO_2\cdot P_2O_5$, and contain much larger amount of P_2O_5 than the bulk slag.

The positions 15 in (a), 14 in (b) and 8 in (c) of the Fig. 2 were identified as the FeO–CaO–SiO_2 melt in which FeO content is high and the ratio of CaO/SiO_2 equals two. These were located adjacent to the $2CaO\cdot SiO_2$ phase. The results of EDS analysis for CS-2, CS-10, CS-20 and CS-30 are plotted as phase diagram for the FeO–CaO–($SiO_2+P_2O_5$) pseudo ternary system in **Fig. 3**. The solid curves indicate the liquidus for the FeO–CaO–SiO_2 system equilibrated with iron at 1 573 K. The plots are classified by solid CaO,

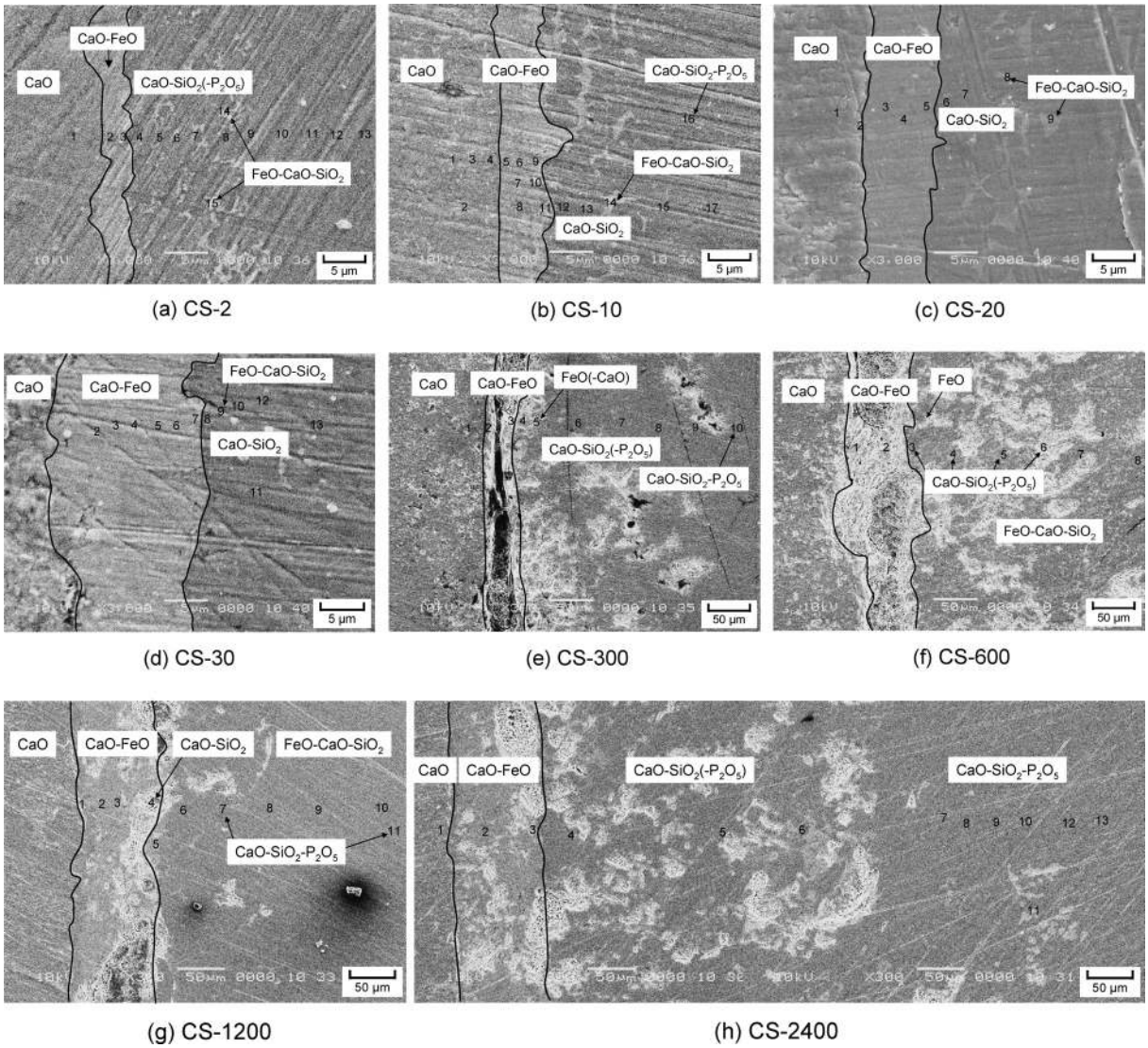

Fig. 2. SEM images for solid CaO and FeO_x–CaO–SiO_2–P_2O_5 slag interface.

CaO–FeO layer, $2CaO \cdot SiO_2$ phase, FeO rich FeO–CaO–SiO_2 phase, $2CaO \cdot SiO_2$ saturated phase and others. In the CaO–FeO layer, high FeO content was observed at position 3 in sample CS-2 and high CaO content was obtained at position 5 in sample CS-10. However, the ratios of CaO/FeO for other positions in CaO–FeO layer almost equal unity. The FeO–CaO–SiO_2 phases that observed adjacent to the $2CaO \cdot SiO_2$ phase are plotted in the $2CaO \cdot SiO_2$ saturated solid and liquid coexisting region. The compositions of high FeO content FeO–CaO–SiO_2 system adjacent to $2CaO \cdot SiO_2$ phase are plotted around liquidus of $2CaO \cdot SiO_2$ saturation. Therefore, it seems that the CaO concentration of the liquid around solid CaO is increased by dissolution of CaO, and composition of the slag reached to the liquidus of $2CaO \cdot SiO_2$ saturation. Then CaO and SiO_2 in the liquid are consumed to form $2CaO \cdot SiO_2$, where the composition of the melt changes along the liquidus and FeO content is increased.

As the thickness of the CaO–FeO layers shown in Figs. 2(a) to 2(h) is obviously increased with reaction time. The thickness of the CaO–FeO layers, $l_{CaO–FeO}$, was measured for every sample from SEM images. The results of measurement of the thickness of the CaO–FeO layer for ten points of each SEM image are shown in **Table 4**. The average thickness is shown as a function of square root of reaction time in **Fig. 4**. A linear relationship exists between the thickness of the CaO–FeO layer and square root of reaction time. This indicates that the growth of the CaO–FeO layer is governed by diffusion of Fe^{2+} ion into solid CaO.

To clarify the formation mechanism of the CaO–FeO layer, it is important to evaluate the activities of FeO and CaO for the CaO–FeO layer, the $2CaO \cdot SiO_2$ saturated slag phase and bulk slag. The activities of the components for the CaO–FeO system at 1 573 K was investigated by Takeda *et al.*[16] In the present study, typical composition of CaO–FeO layer was in the state of solid and liquid coexistence, then the activities of FeO and CaO are equivalent to that of liquidus composition (28mass%CaO–72mass%FeO at 1 573 K). The activity of FeO for 28mass%CaO–72mass% FeO at 1 573 K is reported as 0.48 and that of CaO is 0.84.[16] On the other hand, the activities of FeO and CaO for the FeO_x–CaO–SiO_2–P_2O_5–Al_2O_3 system has not been measured. Therefore, the activities of FeO and CaO for the $2CaO \cdot SiO_2$ saturated slag phase and bulk slag were calculated by using the regular solution model.[17] The activity coefficient of component i in the regular solution model is

expressed by Eq. (3).

$$RT \ln \gamma_i = \sum_j \alpha_{ij} X_j^2 + \sum_j \sum_k (\alpha_{ij} + \alpha_{ik} - \alpha_{jk}) X_j X_k \quad ...(3)$$

where, α_{ij} is interaction energies between i and j, γ_i denotes the activity coefficient of i and X_j does mole fraction of i.

The activity of FeO for the $2CaO \cdot SiO_2$ saturated slag phase was calculated for the compositions of the position 8

Table 2. Results of EDS analysis for samples CS-2 to CS-30 (mass%).

Sample	Position	FeO	CaO	SiO_2	P_2O_5	Al_2O_3
CS-2	1	0.81	99.2	0.00	0.00	0.04
	2	46.7	49.4	0.21	0.00	3.76
	3	79.4	16.5	1.52	0.00	2.53
	4	1.16	62.6	29.2	6.09	0.94
	5	2.39	61.8	30.3	4.72	0.74
	6	47.9	33.9	17.2	0.00	0.93
	7	2.81	63.5	32.2	1.24	0.30
	8	4.08	57.8	25.9	10.3	1.89
	9	2.22	53.0	36.0	4.31	4.46
	10	8.46	42.1	43.1	0.00	6.37
	11	6.51	44.8	30.1	16.1	2.45
	12	13.5	37.4	42.0	2.32	4.80
	13	13.5	38.3	39.8	4.23	4.17
	14	45.6	34.7	19.1	0.00	0.63
	15	89.6	5.75	3.34	0.00	1.29
CS-10	1	0.00	99.7	0.00	0.00	0.29
	2	0.97	98.9	0.00	0.00	0.14
	3	2.56	97.3	0.00	0.00	0.16
	4	3.25	96.2	0.00	0.00	0.50
	5	11.1	87.5	0.00	0.00	1.41
	6	41.1	52.7	1.54	0.00	4.68
	7	33.2	53.2	2.40	0.00	11.2
	8	44.0	49.6	1.49	0.00	4.94
	9	17.8	56.6	15.7	0.00	9.91
	10	36.1	47.8	2.66	0.00	13.5
	11	61.5	33.8	1.21	0.00	3.45
	12	3.41	61.4	32.9	1.77	0.50
	13	1.57	62.7	34.6	1.17	0.00
	14	80.5	10.6	5.61	0.00	3.25
	15	7.76	42.2	40.6	0.00	9.43
	16	3.34	49.9	17.4	27.9	1.45
	17	7.72	44.2	36.1	6.05	5.93
CS-20	1	0.00	100	0.00	0.00	0.00
	2	5.75	94.1	0.00	0.00	0.13
	3	49.2	47.3	1.44	0.00	2.10
	4	47.0	47.6	2.14	0.00	3.33
	5	50.6	43.6	2.60	0.00	3.29
	6	12.5	54.7	30.5	1.49	0.80
	7	7.64	59.6	28.8	3.41	0.56
	8	72.2	15.5	8.79	0.00	3.48
	9	19.4	51.3	24.5	3.95	0.80
CS-30	1	42.7	51.6	2.93	0.00	2.76
	2	43.4	50.3	3.84	0.00	2.45
	3	45.3	48.2	3.95	0.00	2.62
	4	43.9	49.5	3.86	0.00	2.71
	5	44.4	47.2	5.31	0.00	3.09
	6	44.7	48.9	3.33	0.00	3.09
	7	58.0	34.6	5.30	0.00	2.03
	8	2.21	62.1	33.5	1.73	0.40
	9	21.3	50.3	25.5	2.33	0.55
	10	2.15	63.5	31.4	2.95	0.00
	11	1.79	61.0	32.2	4.87	0.21
	12	1.22	63.5	32.3	2.74	0.17
	13	10.8	46.5	36.0	0.19	6.49

Table 3. Results of EDS analysis for samples CS-300 to CS-2 400 (mass%).

Sample	Position	FeO	CaO	SiO_2	P_2O_5	Al_2O_3
CS-300	1	2.21	97.8	0.00	0.00	0.04
	2	57.4	42.3	0.10	0.00	0.21
	3	52.3	43.5	3.76	0.00	0.40
	4	4.63	63.4	31.1	0.71	0.23
	5	96.9	2.74	0.00	0.00	0.31
	6	0.28	65.4	31.3	2.99	0.09
	7	0.64	64.2	31.6	3.49	0.16
	8	7.87	43.8	44.1	0.00	4.25
	9	10.8	44.0	42.1	0.00	3.11
	10	1.80	57.7	14.5	25.6	0.41
CS-600	1	50.8	48.0	1.05	0.00	0.21
	2	51.0	48.2	0.37	0.00	0.43
	3	2.95	64.6	30.1	2.18	0.12
	4	8.27	63.6	26.9	0.97	0.28
	5	0.80	65.6	32.6	0.93	0.04
	6	1.56	60.7	31.8	5.92	0.02
	7	12.3	40.8	44.7	0.00	2.22
	8	1.63	71.4	26.9	0.00	0.00
CS-1200	1	23.7	76.2	0.00	0.00	0.09
	2	51.7	46.5	1.17	0.00	0.59
	3	49.2	48.6	1.28	0.00	0.87
	4	7.87	64.0	27.7	0.00	0.38
	5	53.3	46.4	0.00	0.00	0.26
	6	2.60	63.5	27.1	6.63	0.15
	7	1.12	56.4	14.7	27.6	0.18
	8	21.8	29.2	47.6	0.00	1.41
	9	24.4	28.4	46.0	0.00	1.26
	10	16.7	40.8	30.1	11.6	0.66
	11	8.70	48.3	24.4	18.3	0.25
CS-2400	1	6.94	92.8	0.00	0.00	0.21
	2	51.0	47.0	0.72	0.00	1.27
	3	38.5	56.9	3.42	0.00	1.19
	4	3.45	63.4	30.1	2.94	0.05
	5	1.32	62.8	27.8	7.84	0.22
	6	3.21	62.0	29.7	5.10	0.00
	7	3.17	57.4	17.8	21.5	0.12
	8	12.1	39.0	41.1	0.00	7.83
	9	2.72	56.5	15.6	25.2	0.00
	10	3.61	55.8	16.1	24.3	0.23
	11	3.93	57.9	22.8	15.0	0.35
	12	4.89	54.8	20.5	19.1	0.76
	13	19.4	34.4	43.9	0.00	2.34

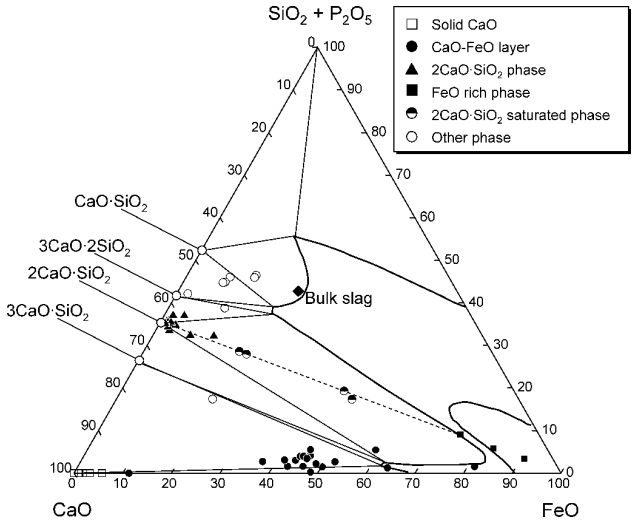

Fig. 3. Results of EDS analysis for sample CS-2, CS-10, CS-20 and CS-30 for the FeO–CaO–(SiO_2+P_2O_5) system.

Table 4. Thickness of CaO–FeO layer.

Sample	Thickness of CaO-FeO layer $\times 10^6$ (m)										Average$\times 10^6$ (m)
CS-2	2.2	2.9	2.7	2.7	3.2	3.1	2.1	2.5	3.2	2.8	2.7
CS-10	8.4	8.7	7.7	7.0	9.0	7.3	8.7	9.7	8.3	8.3	8.3
CS-20	7.0	7.7	8.3	8.3	8.7	8.7	8.0	7.7	7.3	7.0	7.9
CS-30	16.0	16.3	17.0	17.7	17.7	16.3	14.7	13.3	12.7	13.7	15.5
CS-300	39.1	44.9	37.1	32.4	33.2	33.2	3.9	7.0	4.7	43.0	27.9
CS-600	66.4	66.4	78.1	70.3	69.5	78.1	50.8	50.8	46.9	56.6	63.4
CS-1200	85.9	84.0	78.1	76.2	64.5	84.0	78.1	84.4	84.0	85.9	80.5
CS-2400	82.0	84.0	80.1	84.0	85.9	82.0	82.0	83.2	80.1	78.1	82.1

of sample CS-20, because this composition is the liquidus composition shown in Fig. 3 and that for bulk slag was calculated for the result of analysis for pre-melted slag PR-3 in Table 1. The results of calculation for the activities of FeO and CaO by the regular solution model are shown in **Table 5** together with the results for CaO–FeO layer. The activity of FeO for the $2CaO \cdot SiO_2$ saturated slag phase is larger than that for the CaO–FeO layer and bulk slag. Then Fe^{2+} ion diffuses from $2CaO \cdot SiO_2$ saturated phase to both the CaO–FeO layer and bulk slag. In addition, the activity of CaO for CaO–FeO layer is much larger than that for the

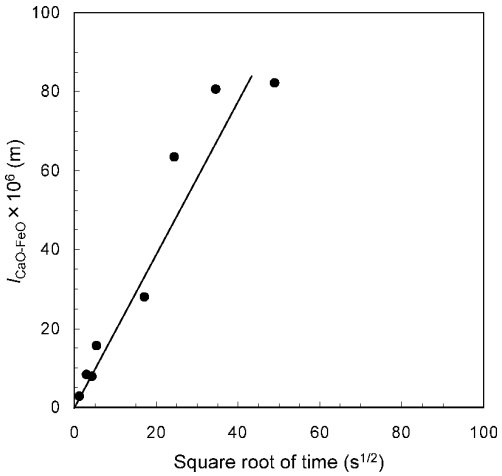

Fig. 4. Relationship between thickness of the CaO–FeO layer and reaction time.

Table 5. Evaluation of activities of FeO and CaO.

Sample	Phase	Activity of FeO	Activity of CaO
—	CaO-FeO	0.48	0.84
PR-3	Bulk slag	0.27	0.0020
CS-20, position 8	$2CaO \cdot SiO_2$ saturated slag	0.85	0.0049

$2CaO \cdot SiO_2$ saturated FeO–CaO–SiO_2 phase and bulk slag. Therefore, the activity gradient of CaO leads to diffusion of Ca^{2+} ion from solid CaO to bulk slag through CaO–FeO layer. Consequently, it is assumed that the formation mechanism of CaO–FeO layer are caused by the activity gradient of FeO between the CaO–FeO layer and the $2CaO \cdot SiO_2$ saturated melt. If CaO–FeO layer were formed beside solid CaO, Ca^{2+} ion would diffuse from solid CaO toward bulk slag continuously. Then CaO–FeO layer and $2CaO \cdot SiO_2$ saturated region grow and dissolution of CaO into slag proceeds.

The reaction mechanism of solid CaO and FeO_x–CaO–SiO_2–P_2O_5 slag at 1 573 K is considered to be as follows.

(1) Solid CaO dissolve into the slag and content of CaO in the melt increases. (**Fig. 5**(a))
(2) $2CaO \cdot SiO_2$ is formed in the melt, so CaO and SiO_2 are consumed and the content of FeO in the slag increases. (Fig. 5(b))
(3) According to the activity gradient of FeO, Fe^{2+} diffuses from FeO rich phase to both solid CaO and bulk slag. (Fig. 5(c))
(4) CaO–FeO layer is formed beside solid CaO. (Fig. 5(d))
(5) Ca^{2+} diffuses toward bulk slag phase through the CaO–FeO layer. (Fig. 5(e))

4. Conclusion

The reaction mechanism of solid CaO and FeO_x–CaO–SiO_2–P_2O_5 slag at 1 573 K is determined by the observation and analysis of the reaction between solid CaO and liquid slag. The mechanism of the reaction is described as (1) Solid CaO dissolve into the slag and content of CaO in the melt increases. (2) $2CaO \cdot SiO_2$ is formed in the melt, so CaO and SiO_2 are consumed and the content of FeO in the

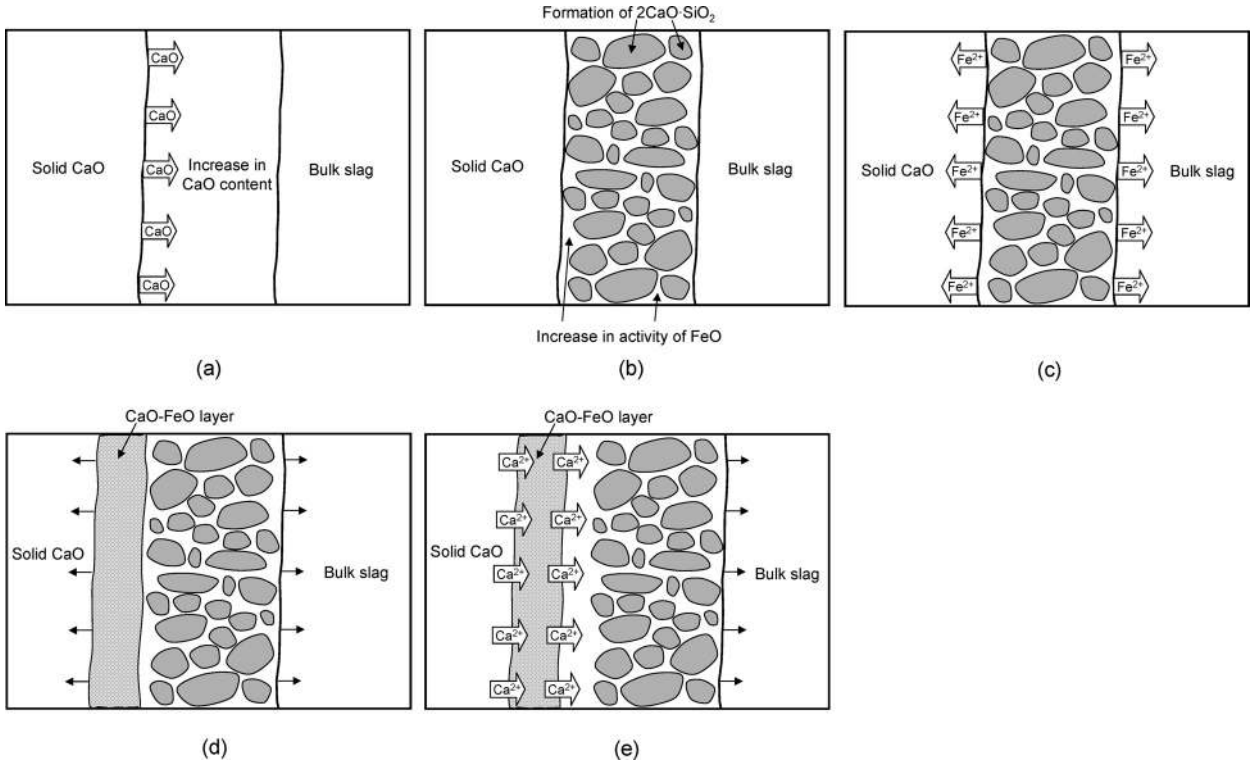

Fig. 5. Schematics of reaction mechanisms.

slag increases. (3) According to the activity gradient of FeO, Fe_{2+} diffuses to both solid CaO and bulk slag. (4) CaO–FeO layer is formed beside solid CaO.

REFERENCES

1) W. J. Schlitt and G. W. Healy: *Am. Ceram. Soc. Bull.*, **50** (1971), 954.
2) V. R. Scheel and F. Oeters: *Arch. Eisenhüttenwes.*, **42** (1971), 769.
3) V. L. Hachtel, W. Fix and G. Trömel: *Arch. Eisenhüttenwes.*, **43** (1972), 361.
4) T. Onoye, T. Ishii, K. Uemura and K. Narita: The 4th Japan-USSR Joint Symp. on Phys. Chem. of Metall. Proc., ISIJ, Tokyo, (1973), 100.
5) H. Kimura, T. Yanagase, F. Noguchi and Y. Ueda: *J. Jpn. Inst. Met.*, **38** (1974), 226.
6) F. Oeters and R. Scheel: *Arch. Eisenhüttenwes.*, **45** (1974), 575.
7) M. Matsushima, S. Yadoomaru, K. Mori and Y. Kawai: *Tetsu-to-Hagané*, **62** (1976), 182.
8) F. Noguchi, Y. Ueda and T. Yanagase: *J. Jpn. Inst. Met.*, **41** (1977), 883.
9) C. A. Natalie and J. W. Evans: *Ironmaking Steelmaking*, (1979), 101.
10) H. Ono, T. Masui and H. Mori: *Tetsu-to-Hagané*, **69** (1983), 1763.
11) M. H. Chiang, G. I. Yang, H. Y. Chang, T. F. Lee and R. DasGupta: *Am. Ceram. Soc. Bull.*, **67** (1988), 1222.
12) H. Sunayama, M. Kawahara, T. Kozuka, T. Mitsuno and Y. Mizukami: Proc. of Molten Slags, Fluxes and Salts '97 Conf., ISS, Warrendale, PA, (1997), 613.
13) P. Koopmans, A. van Belzen and B. Snoeijer: Proc. of Molten Slags, Fluxes and Salts 2000 Int. Conf., CD-ROM, RIT, Stockholm, (2000), 095.pdf.
14) E. T. Turkdogan: Physical Chemistry of High Temperature Technology, Academic Press, New York, (1980), 5.
15) Verein Deutscher Eisenhuttenleute: SLAG ATLAS, 2nd Ed., Verlag Stahleisen GmbH, D-Düsseldorf, (1995), 57.
16) Y. Takeda and A. Yazawa: *J. Min. Metall. Inst. Jpn.*, **96** (1980), 901.
17) S. Ban-ya: *ISIJ Int.*, **33** (1993), 2.